

Effect of cooling rate on the post-fire behavior of CFST column

Alireza Afaghi-Darabi^a and Gholamreza Abdollahzadeh^{*}

Department of Civil Engineering, Babol Noshirvani University of Technology, Shariati Av., Babol, Mazandaran, Iran

(Received November 9, 2018, Revised March 22, 2019, Accepted March 30, 2019)

Abstract. The post-fire behavior of structural elements and the cooling process has always been one of the main concerns of the structural engineers. The structures can be cooled at different rates, where they affect the structure's behavior. In the present study, a numerical model has been developed using the Abaqus program to investigate the effect of cooling rate on the post-fire behavior of the CFST column. To verify the model, results of an experimental study performed on CFST columns within a full heating and cooling cycle have been used. In this model, comparison of the residual strength has been employed in order to examine the behavior of CFST column under different cooling rates. Furthermore, a parametric study was carried out on the strength of steel and concrete, the height of the specimens, the axial load ratio and the cross-sectional shape of the specimen through the proposed model. It was observed that the cooling rate affects the behavior of the column after the fire, and thus the higher the specimen's temperature is, the more effect it has on the behavior. It was also noticed that water cooling had slightly more residual strength than natural cooling. Furthermore, it was recognized from the parametric study, that by increasing the strength of steel and concrete and the load ratio, as well as modifying the cross-sectional shape from circular to square, residual strength of column at the cooling phase was less than that of the heating phase. In addition, with reducing column height, no change was witnessed in the column behavior after the cooling phase.

Keywords: water cooling; Natural cooling; cooling rate; post-fire; residual strength

1. Introduction

Fire, as well as earthquake, is one of the possible events that have to be considered when the structure is designed. Unlike earthquakes, which is a natural occurrence, fire is one of the events in which human being is also involved. On the one hand, it is presumed that fire can be prevented due to the everyday increase of safety issues. However, by looking at daily happenings, it is observed that fire in structures, still takes the lives of people. On the other hand, considering the effect of the human factor on fire, as more people live in a building, the possibility of fire will also increase. This issue becomes more important given the increase in population and the limitation of urban space and, consequently, the increase of high-rise buildings.

With the development of high-rise buildings, it is necessary to use elements with high construction speed, stiffness and strength, good seismic behavior and high fire resistance; while all these features are comprehensively incorporated in the CFST column. These columns have better ductility than concrete columns because of the confinement of concrete. Likewise, their stiffness and fire resistance are much higher than steel columns, and the construction speed is greater than that of concrete columns. Consequently, this type of column is widely used in high-rise buildings in high seismic areas (Gourley *et al.* 2001).

Considering the widespread use of CFST columns in structures and the necessity of considering fire in the design of such structures, the behavior of CFST column under fire is very important. The behavior of the concrete and steel widely have been studied. In the past, the behavior of concrete (Ozbolt *et al.* 2008, Ibrahimbegovic *et al.* 2010, Guergah 2017, Liang *et al.* 2017, Liang *et al.* 2018, Dimia, *et al.* 2018) and steel (Outinen and Mäkeläinen 2004, Chen *et al.* 2006) and steel-concrete composite columns (Dimia *et al.* 2017) against fire has been widely studied. The fire resistance of concrete against fire is more than steel, but the construction rate of steel structures is greater. In the CFST column, using both of these materials, their weaknesses are eliminated. Recently, extensive research has been carried out on the CFST column's behavior under fire (Lie 1994, Sakumoto *et al.* 1994, Han 2001, Han *et al.* 2003, Yu *et al.* 2010, Yang *et al.* 2013, Abdollahzadeh and Afaghi 2017, Abdollahzadeh and shalika 2017, Peng *et al.* 2017, Tan *et al.* 2018).

Yet, the critical point is that if the column is not ruptured during the fire, its post-fire behavior is very important. Whether this column needs rehabilitation or should it be demolished? Can it be used without repair? There are still other questions that make it very important to explore the post-fire behavior of the column. Numerous researches have also been done on the behavior of the reinforced concrete and CFST column after the fire (Gernay and Dimia 2011, 2013, Han *et al.* 2002, Yang *et al.* 2008, Song *et al.* 2010, Yao and Hu 2015). It might be conceived at first that by cooling the specimen, its strength will slightly decrease compared to the initial value, or that it stays constant at the same amount of strength at maximum temperature.

*Corresponding author, Ph.D.

E-mail: Abdollahzadeh@nit.ac.ir

^aM.sc.

E-mail: Alireza.afaghi@stu.nit.ac.ir

However, the internal temperature of the concrete will increase during the cooling phase due to concrete's low heat transfer coefficient, resulting in a reduction in the strength of the concrete. On the other hand, the strength of steel will increase because of the decrease in temperature. As a result, the behavior of the CFST column will be very complicated during the cooling phase.

In order to evaluate the behavior of the column in the full range of heating and cooling, a numerical model has been performed by Dimia *et al.* (2011) to study on the collapse of reinforced concrete columns subjected to natural fire conditions during and after the cooling phase of the fire. Also, Yang (2008) was developed a numerical model to predict the behavior of the CFST column, though in this model there is a complete bond between steel and concrete which is not the correct assumption. Yi-Song (2010) has provided another numerical model to predict the behavior of the CFST column considering the initial load effect.

Nevertheless, in all these models, the validation of these specimens was done separately because of the lack of experimental data until then, implying that for each of the heating, cooling, and post-fire stages, a separate verification was implemented. A parametric study was also conducted to study the CFST column's behavior more accurately.

What indeed happens after the fire is that the firefighters try to put quickly off the fire with different water jets. At first glance, this seems desirable, yet in experimental investigations by Abramowicz and Kowalski (2005), it was found that the concrete behavior varies under different cooling rates, and thus its strength decreases by increasing the rate due to the formation of micro-cracks in concrete.

To compare the behavior of the CFST column in cases of water and natural cooling, Abbas *et al.* (2017), conducted an experimental study on 30 different CFST and CFDST specimens under different loading conditions. The result of this experiment was that the natural cooling of the specimens had a slightly better effect than the water cooling. Due to the importance of Post-fire residual strength of structural elements and the effect of cooling rate on it, it is necessary to study the Post-fire behavior of the CFST columns more precisely.

Because of the cost of an experimental study on the CFST column under a full range of heating and cooling and post-fire phase to assess the parameters affecting it, a numerical modeling is preferable. But numerical modeling should be sufficiently precise, and this is accepted with valid verification. However, numerical models have been presented so far such as Huo *et al.* (2009) model, which is the stage Cooling is not considered or Espinos *et al.* (2017), Wang *et al.* (2011), Song *et al.* (2010), Yang *et al.* (2008) that due to the lack of experimental data until then, which put the CFST column under a full range of heating and cooling and post-fire phase, verifications are performed separately, That is, each heating and cooling stage was individually verified, while this method reduces the accuracy of the model because the model must have the capability to transfer the damage from the heating stage to the cooling stage and then, but the verification of the papers mentioned does not support the model's ability.

In the model presented in this study, the experimental data provided by Abbas *et al.* (2017) is used to verify the

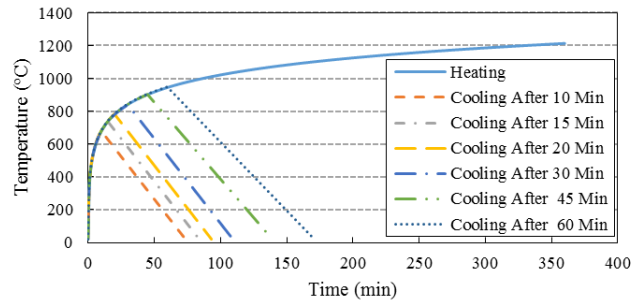


Fig. 1 Natural cooling curve

model, in which the CFST column is placed under a complete heating and cooling range. The obtained results confirm the model's accuracy in transferring damage from the heating stage to the cooling stage. Then, using this model, a parametric study was performed and the effect of different parameters was investigated.

When the CFST column is exposed to fire, the temperature distribution in the concrete cross-section will be non-uniform due to the low thermal conductivity of concrete. Therefore, after the fire and during the cooling phase, each point in the cross-section experiences a certain maximum temperature. In order to consider this mode in the model, the cross-section of the concrete is considered to be layered. Then using the parametric study, the effect of various factors including loading ratio, the strength of the material, height of specimen and cross-sectional shape have been investigated on the column residual strength.

2. Numerical model

2.1 General

In this study, a numerical model has been developed using ABAQUS program. Using the comparison of the residual strength curve of the column, the effect of cooling rate on the behavior of CFST column is obtained considering the entire fire cycle, namely heating, cooling, and Post-fire phases. The ISO-834 standard fire curve (Song *et al.* 2010) has been used to apply fire at the heating phase. Likewise, the relation in Appendix A of EN1991-1-2 (2002) has been used to apply natural cooling conditions.

In this model, each specimen has been exposed to fire for a specific amount of time before the failure. The temperature increase was then stopped, thus entering the Cooling Phase. In the case of natural cooling, temperature reduction is applied to the specimen according to Eq. (1) base on Appendix A of EN1991-1-2 (2002), but in case of water cooling, while natural cooling has the lowest cooling rate, the most critical condition is used for considering the highest cooling rate; since the purpose of this paper is to investigate the effect of different cooling rates.

$$\begin{cases} T=T_h-10.417(t-t_h) & t_h \leq 30 \text{ min} \\ T=T_h-4.167\left(3-\frac{t_h}{60}\right)(t-t_h) & 30 < t_h < 120 \text{ min} \\ T=T_h-4.167(t-t_h) & t_h \geq 120 \text{ min} \end{cases} \quad (1)$$

Where:

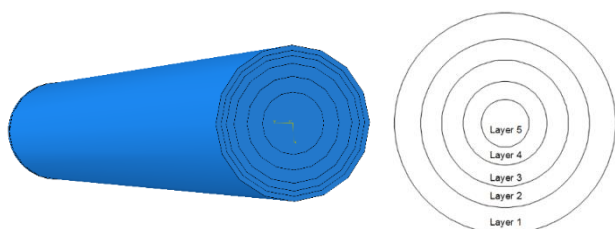


Fig. 2 Layered CFST section in F.E. model

T =fire temperature in $^{\circ}\text{C}$.

t = fire exposure time in min.

t_h =fire duration time in min.

T_h =maximum fire temperature in $^{\circ}\text{C}$.

It is assumed that the temperature of the outer surface of steel suddenly reaches 20 degrees. During the cooling phase, the rise in the temperature will continue within the concrete. The reason of this phenomenon is the low thermal conductivity of concrete, which causes a non-uniform distribution of cross-sectional temperature. Assume that the concrete specimen in Fig. 2 is exposed to fire. The temperature of layer 1 increase, then the temperature of layer 2 increases. This process continues until the temperature of layer 5 increases. If the fire stops and the specimen entered the cooling stage, Firstly, the temperature of the layer 1 decrease. To reduce the temperature of the layer 2, the temperature of the layer 1 must be lowered than the layer 2. While the layer 1 is cooling down, the layer 2 is still transferring the heat (which obtained from the heating stage) to the coolest layers of 3, 4 and 5. This procedure will occur for layers 3, 4, 5. Therefore, during this time the temperature of the internal layers increases. As a result, a more realistic output is gained by using layered column section as shown in Fig. 2. The maximum temperature experienced by the points on the cross section is then calculated separately in the Heat transfer analysis to be used in subsequent steps.

Additionally, to consider the effect of the interaction between inner surface of steel and outer surface of concrete, the model provided by Coulomb has been used so that the "hard contact" is used in the normal direction which allows the two surfaces to be separated, though not allowed to pass through each other in compression. The Coulomb friction coefficient of 0.3 is used in tangent direction.

To make the axial load divided proportional to the cross-sectional area and stiffness of steel and concrete, a plate is used above the steel tube and concrete. In other words, to ensure that the load applied to the top of the column is actually distributed in accordance with the experimental conditions between steel and concrete, a plate is to be placed at the top of the column. So, when the fire is not applied, the composite load is applied between the steel and the concrete (due to their cross-sectional strength and stiffness), and when the fire is applied before the yielding of steel tube, due to the high thermal expansion of the steel, which causes the steel tube is detached from the concrete in the direction of the height, this plate applies the load correctly to steel only.

The DC3D8 Continuum Solid element is used for steel tube, concrete core and the cap plate. Also, the mesh

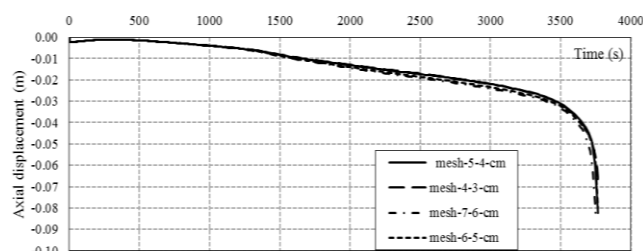


Fig. 3 Fire resistance of Specimens with different mesh sizes

dimensions were investigated using mesh sensitivity analysis on the axial deformation of specimens until the failure and its appropriate dimensions were obtained. The result of mesh sensitive analysis illustrated in Table 1 and in Fig. 3.

The boundary conditions considered for specimens were Fixed-Fixed for both ends, in which the upper part was released for axial displacement. The temperature distribution of the columns and its mechanical behavior are calculated respectively via the heat transfer and the stress analyses. To calculate the residual strength of the specimens in the Post-fire phase, the axial load is gradually increased until the specimens are ruptured. The failure criterion according to BS-476 (1987) is when the axial deformation or its rate of change, respectively exceed $L/20$ or $L^2/9000 D$ (in mm/min), (D is the diameter (in mm) and L is the length of the column (in mm)) each happens earlier.

2.2 Thermal analysis

The thermal properties of concrete and steel at the heating stage including the specific heat and thermal conductivity are obtained according to lie, t , t (1995) According to Schneider's (1985), it was found that, during the heating phase, the moisture content of the concrete is lost, and the thermal properties of the concrete including specific heat, thermal conductivity, and the density depending on the moisture content of the concrete.

These parameters in the cooling stage do not change and depend on the maximum temperature of the various points of the concrete cross-section (Dimia *et al.* 2011). But in the case of steel, all of its properties are assumed to return to its original state at ambient temperature. To obtain the maximum temperature, the specimen is layered, the maximum temperature is obtained in each layer at the end of the heating phase. It should also be noted that the number of layers is determined according to the variation of temperature at the cross-section of the concrete. The values of convection and emissivity are also 25 ($\text{W}/\text{m}^2 \text{K}$) and 0.5 for the external surface of steel, respectively (Ding and Wang 2008). Moreover, in order to take the thermal resistance (Zhang *et al.* 2011) between steel and concrete into account, the relationship provided by Ghajel (2004) has been used according to Eq. (2).

$$h_j = a_1 - b_1 \exp(-cT^d) \quad \text{W}/\text{m}^2\text{C} \quad (2)$$

$$a_1 = 160.5, b_1 = 63.8, c = 339.9, d = -1.4, T = \text{Temperature } (^{\circ}\text{C})$$

Table 1 Specimen details

| Specimens | concrete mesh size (cm) | Steel tube mesh size (cm) | Number of node | Fire resistance (s) |
|-----------|-------------------------|---------------------------|----------------|---------------------|
| 1 | 7 | 6 | 7599 | 3750 |
| 2 | 6 | 5 | 10218 | 3765 |
| 3 | 5 | 4 | 14122 | 3763 |
| 4 | 4 | 3 | 23435 | 3766 |

2.3 Material properties

Concrete damage plasticity model has been used to consider the plastic behavior of concrete. The mechanical properties used for concrete and steel in different phases of temperature change are as follows.

a) Heating phase

$$\sigma_s = \begin{cases} \frac{f(T, 0.001)}{0.001} \varepsilon_s & \varepsilon_s \leq \varepsilon_p \\ \frac{f(T, 0.001)}{0.001} \varepsilon_p + f[(T, (\varepsilon_s - \varepsilon_p + 0.001))] & \varepsilon_s > \varepsilon_p \\ -f(T, 0.001) & \varepsilon_s > \varepsilon_p \end{cases} \quad (3)$$

In the heating phase, the stress-strain relationship of Lie and Chabot (1992) have been used for steel.

So that $\varepsilon_p = 4 \times 10^{-6} f_y$, $f(T, x) = (50 - 0.04T) \times \{1 - \exp[-30 + 0.03T] \sqrt{x}\} \times 6.9$
 $T = \text{Temperature } (^{\circ}\text{C})$

$$y = \begin{cases} 2x - x^2 & x \leq 1 \\ \beta_0(x - 1)^\eta + x & x > 1 \end{cases} \quad (4)$$

For confined concrete, Song (2010) relations are used at the heating stage.

So that $x = \frac{\varepsilon_c}{\varepsilon_{oh}}$, $y = \frac{\sigma_c}{\sigma_{oh}}$

$\sigma_{oh} = \text{Peak concrete stress at temperature } T = fc / [1 + 1.986 \cdot (T - 20)^{3.21} \times 10^{-9}]$

$\varepsilon_{oh} = \text{Peak concrete strain at temperature } T = (1300 + 12.5)f_c + 800\xi^{0.2} \cdot 10^{-6} (1.03 + 3.6 \times 10^{-4}T + 4.22 \times 10^{-6}T^2)$

$$\eta = \begin{cases} 2 & \text{concrete-filled CHS} \\ 1.6 + 1.5/x & \text{concrete filled SHS and RHS} \end{cases} \quad (5)$$

$$\beta_0 = \begin{cases} (2.36 \times 10^{-5})^{[0.25 + (\xi - 0.5)^7]} (f_c^{0.5}) \times 0.5 \geq 0.12 & \text{(concrete-filled CHS)} \\ \frac{(f_c)^{0.1}}{1.2\sqrt{1 + \xi}} & \text{(concrete-filled SHS and RHS)} \end{cases} \quad (6)$$

$$\xi = \text{confinement factor} = \frac{A_s f_y(T)}{A_c f_{ck}} \quad (7)$$

$$f_{yh}(T) = \begin{cases} f_y & T < 200^{\circ}\text{C} \\ \frac{0.91 f_y}{(1 + 6 \times 10^{-17}(T - 10)^6)} & T \geq 200^{\circ}\text{C} \end{cases} \quad (8)$$

$f_{ck} = \text{Characteristic concrete strength (MPa)}$

$fc = \text{Concrete cylinder compressive strength (MPa)}$

$f_y = \text{Yield strength (in MPa) of steel at ambient temperature}$

$f_y(T) = \text{Yield strength (in MPa) of steel at temperature } T$

Also, the modulus of elasticity of concrete is obtained from Anderberg & the Anderson (1976) as follows.

$$E_{cT} = \frac{2 \times f_{cT}}{\varepsilon_{0T}} \quad (9)$$

$f_{cT} = \text{Concrete compressive strength at temperature } T \text{ (MPa)}$

Lie, *t*, *t* (1995) is also used for the thermal expansion coefficient of steel and concrete.

b) Cooling phase

In the cooling phase, the properties of steel are in accordance with Yang *et al.* (2008). Using this relation, in order to obtain the steel properties at any given moment in the cooling phase, a linear interpolation relation is used between its respective values at maximum temperature and ambient temperature (20°C).

$$\sigma_s = \begin{cases} E_{sc}(T, T_{max}) \cdot \varepsilon_s & \varepsilon_s \leq \varepsilon_{yc}(T, T_{max}) \\ f_{yc}(T, T_{max}) + 0.01 E_{sc}(T, T_{max}) \cdot \varepsilon_s & \varepsilon_s > \varepsilon_{yc}(T, T_{max}) \end{cases} \quad (10)$$

$$f_{yc}(T, T_{max}) = f_y(T_{max}) - \frac{T_{max} - T}{T_{max} - T_0} \times [f_y(T_{max}) - f_{yp}(T_{max})] \quad (11)$$

$$\varepsilon_{yc}(T, T_{max}) = \varepsilon_y(T_{max}) - \frac{T_{max} - T}{T_{max} - T_0} \times [\varepsilon_y(T_{max}) - \varepsilon_{yp}(T_{max})] \quad (12)$$

$$E_{sc}(T, T_{max}) = \frac{f_{yc}(T, T_{max})}{\varepsilon_{yc}(T, T_{max})} \quad (13)$$

Stress-strain relationship of steel in the cooling phase:

$E_s = \text{young's modulus of steel at ambient temperature} = 206000 \text{ MPa}$

$$\varepsilon_{yp}(T_{max}) = \frac{f_{yp}(T_{max})}{E_s} \quad (14)$$

$$\varepsilon_{yp}(T_{max}) = \frac{f_{yp}(T_{max})}{E_s} \quad (15)$$

$$f_{yp}(T_{max}) = f_y \times \begin{cases} 1 & T_{max} \leq 400^{\circ}\text{C} \\ 1 + 2.33 \times 10^{-4}(T_{max} - 20) - 5.88 \times 10^{-7}(T_{max} - 20)^2 & T_{max} > 400^{\circ}\text{C} \end{cases} \quad (16)$$

$$\xi = \text{Post - fire confinement factor} = \frac{A_s f_{yp}(T_{max})}{A_c f_{ck}}$$

$f_{yp}(T_{max}) = \text{Post-fire yield strength (in MPa) of the steel at temperature } T_{max}$

$f_y = \text{Yield strength (in MPa) of steel at ambient temperature}$

$f_{cT} = \text{Concrete compressive strength (in MPa) at temperature } T$

$f_y(T) = \text{Yield strength (in MPa) of steel at temperature } T$

In the case of concrete, similar to the assumption made by Yang *et al.* (2008), the properties are not changed at the cooling phase and do not depend on the temperature of each

moment in the cooling phase. In other words, the properties of concrete at any moment in the cooling phase is equal to its properties after cooling and reaching the ambient temperature.

c) Post-fire phase

In the post-fire phase, the steel and the confined concrete properties are presented in accordance with Yang *et al.* (2008).

For steel:

$$\sigma_s = \begin{cases} E_s \cdot \varepsilon_s & \varepsilon_s \leq \varepsilon_{yp}(T_{max}) \\ f_{yp}(T_{max}) + 0.01E_s \cdot [\varepsilon_s - \varepsilon_{yp}(T_{max})] & \varepsilon_s > \varepsilon_{yp}(T_{max}) \end{cases} \quad (17)$$

$$\varepsilon_{yp}(T_{max}) = \frac{f_{yp}(T_{max})}{E_s} \quad (18)$$

$$\begin{cases} 1 & T_{max} \leq 400^\circ C \\ 1 + 2.33 \times 10^{-4}(T_{max} - 20) - 5.88 \\ \times 10^{-7}(T_{max} - 20)^2 & T_{max} > 400^\circ C \end{cases} \quad (19)$$

$$\xi = \text{Post-fire confinement factor} = \frac{A_s f_{yp}(T_{max})}{A_c f_{ck}} \quad (20)$$

Also for concrete, according to Song *et al.* (2010), the stress-strain curves were in accordance with Eq. (4) with the Peak stress and peak strain as follows

$$\begin{aligned} \sigma_{ocp} &= f_c / [1 + 2.4 \cdot (T_{max} - 20)^6 \times 10^{-17}] \\ \varepsilon_{ocp} &= (1300 + 12.5f_c) \times 10^{-6} \\ &\times [1 + (1500 T_{max} + 5 T_{max}^2) \times 10^{-6} \\ &+ 800\xi^2 \times 10^{-6}] \end{aligned} \quad (21)$$

f_c = Concrete cylinder compressive strength (MPa)

$f_{yp}(T_{max})$ = Post-fire yield strength (in MPa) of the steel at temperature T_{max}

E_s = Steel modulus of elasticity (MPa)

f_y = Yield strength (in MPa) of steel at ambient temperature

$f_y(T)$ = Yield strength (in MPa) of steel at temperature T

3. Verification

In order to validate the model, experimental data provided by Abbas *et al.* (2017) have been used. In this study, an experimental study was carried out on 30 different CFST and CFDST specimens under entire temperature cycle including heating, cooling and post-fire phase. Given



Fig. 4 Column specimens after taking out from the oven (Abbas *et al.* 2017)

that only data on the load-displacement curve of the specimens are extracted from Abbas's study, and there are no temperature data, therefore in this work, only the output of the load-displacement curve is compared with the numerical model presented in this study. All three specimens have boundary conditions of Fixed-Fixed for both ends. The axial load of all specimens is 170 newton. This value, as illustrated in Fig. 4, is the load caused by the concrete block on the top of the specimens during heating phase. In the verification model, in order to consider the effect of the initial geometric imperfection, which is due to the initial distortion in the structural element, the buckling analysis is performed on the specimen and the first buckling mode is obtained. This effect is applied to the model by multiplying the displacements of points of this mode shape in $L/1000$ (L is the length of the column (in m)). The details of the specimens are reported in Table 2.

In this experimental study, as shown in Fig. 4, the specimens were first exposed to temperature $600^\circ C$ for 3 hours to reach a uniform surface temperature. Then the specimen was placed in ambient temperature for 24 hours. After the specimen is cooled, using the AMSLER compression testing machine, a displacement at a rate of 0.25 (mm/s) is applied to break the specimens. The output of this experiment is the load-axial deformation curve of specimens, which is compared with the model presented in this paper. Two types of loading methods have been carried out in this experiment. In the "Composite Loaded" method, the load is applied to both steel and concrete, and in the "Core loaded" method, the load is only applied to concrete. Moreover, in specimen S3, there is no concrete inside the tube and thus the steel tube is merely investigated.

To model this column in Abaqus program, a buckling analysis is first performed to take into account the effects of the initial geometric imperfection. Then, heat transfer analysis is carried out to determine the temperature of the

Table 2 Details of specimens for verification.

| Specimens | Outer diameter (mm) | Thickness (mm) | Height (mm) | Concrete compressive strength (MPa) | Steel yield Stress (MPa) | Loading type |
|-----------|---------------------|----------------|-------------|-------------------------------------|--------------------------|------------------|
| S1 | 150 | 6 | 600 | 40 | 307 | Composite loaded |
| S2 | 150 | 6 | 600 | 40 | 307 | Core loaded |
| S3 | 112.5 | 4 | 450 | - | 307 | Composite loaded |
| S4 | 112.5 | 4 | 450 | 40 | 307 | Core loaded |

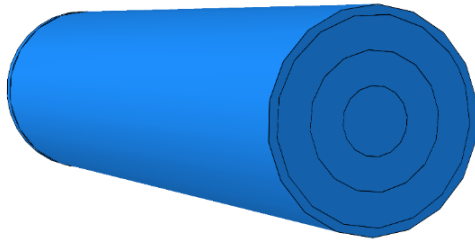


Fig. 5 Layered CFST specimen in FE model for verification

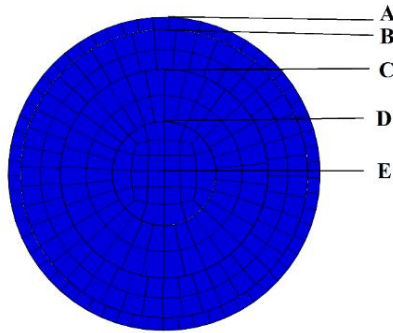


Fig. 6 Specimens cross-section

Table 3 Temperature of the points

| Points | Distance from center (mm) | Temperature after 3 hours (°C) |
|--------|---------------------------|--------------------------------|
| A | 75 | 591.5 |
| B | 69 | 582.7 |
| C | 46 | 567.2 |
| D | 23 | 560.5 |
| E | 0 | 560 |

various points of the column at any moment. Finally, a general static analysis is performed to investigate the mechanical behavior of the CFST column. In the model presented in this paper, the properties of steel and concrete were also according to the properties provided in Section 2 in the heating, cooling and post-fire phases. In this model, the temperature at different points of the column will be uniform, given that the specimen is exposed to temperature 600°C for 3 h. However, to increase accuracy, as seen in Fig. 5, concrete cross-section is layered into three different parts. Also in Fig. 6 and Table 3, the Temperature distribution is observed on the cross-section of the column after 3 hours.

Because of the uniformity of the temperature of the points in the cross-section, only 3 layers were selected. After the natural cooling phase is started, the outer layers begin to cool down through the inner layers are cooled at a lower rate. In order To verify the validity of the presented model, the load-axial deformation curve of specimens is compared with each other.

As can be seen from Fig. 7, there is a good agreement between experimental and numerical results. There is however a slight difference which can be due to errors in the laboratory’s measurement systems or errors arising in the testing process. As a result, this model can be used for further investigation of the CFST column.

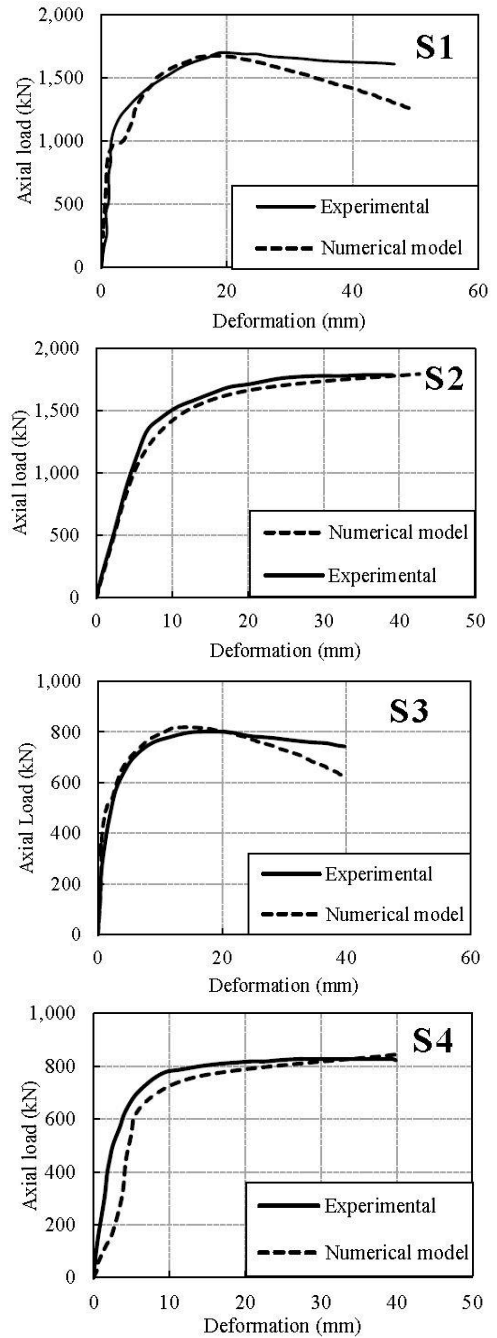


Fig. 7 Comparison of load-deformation curve between experimental and numerical result for verification

4. CFST column behavior under different rates of cooling

In this section, using a validated model, the behavior of the CFST column is evaluated after a full range of heating, cooling and once the cooling rate is inclusive of various values. The lowest rate of cooling is assumed to be in the natural state, so that the specimens are exposed to air, to reach a temperature of 20°C. In this model, the specimen is exposed to ambient temperature for 24 hours to reach a uniform temperature of 20°C.

In order to take into account the highest rate of cooling, the most critical possible state, in which the temperature of

Table 4 Details of the specimens in the model.

| Specimens | Shape | Section size (mm) | Thickness (mm) | Load ratio | Load (kN) | Concrete compressive strength (MPa) | Steel yield strength (MPa) | Height (mm) |
|-----------|--------|-------------------|----------------|------------|-----------|-------------------------------------|----------------------------|-------------|
| C1 | square | 300*300 | 6 | 0.5 | 2419.2 | 40 | 307 | 3200 |
| C2 | square | 300*300 | 6 | 0.5 | 1858.6 | 30 | 240 | 3200 |
| C3 | circle | 300(Diameter) | 10 | 0.5 | 2433.7 | 40 | 307 | 3200 |
| C4 | square | 300*300 | 6 | 0.5 | 2474.4 | 40 | 307 | 1600 |
| C5 | square | 300*300 | 6 | 0.35 | 1693.4 | 40 | 307 | 3200 |

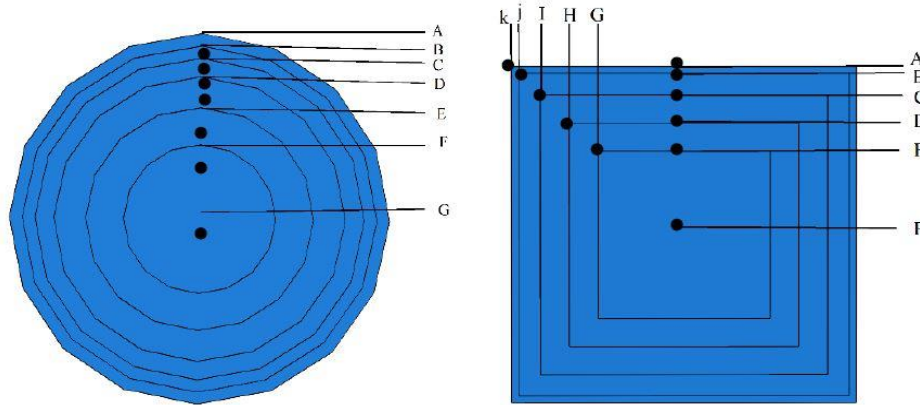


Fig. 8 The cross-sectional shape of the specimens

the external surface suddenly reaches 20 degrees is considered. The details of the specimens in this section are in accordance with Table 4.

4.1 Temperature distribution

The temperature distribution of different points of the column is obtained using the Heat transfer analysis. The procedure for applying the cooling conditions is the same as that described in section 2.2. After determining the maximum temperature of the different points and according to the temperature distribution, the section is layered and the maximum temperature is determined for each layer in accordance with Table 5 and Table 6, Table 7 and Table 8. In order to determine the maximum temperature of each layer at a square cross-section, the average temperature of points in the corner and the middle of each side is considered in both outer and inner parts of the layer. For example, the temperature of the layer 2 is calculated

$$\text{Layer 2 (square section): } T_{\max} = \frac{T_B + T_c + T_j + T_l}{4} \quad (22)$$

$$\text{Layer 2 (circular section): } T_{\max} = \frac{T_B + T_c}{2}$$

T =Temperature ($^{\circ}C$)

It should be noted that the maximum temperature of the points in the concrete does not correspond to the initiation of the cooling phase, while after the cooling phase begins, the internal points of the concrete still continue to increase in temperature. As a result, the maximum temperature will always take place shortly after the cooling phase starts. The layering of the specimens reported in Table 4 is shown in Fig. 8. It should be noted that Layer 1 is a steel tube. Since the specimens C1, C2, C4, and C5 have a similar cross-section, the layering and temperature distribution are

similar. In the case of natural cooling, the maximum temperature of the specimens is shown in Tables 5-6 and in the case of water cooling, the maximum temperature obtained from the specimens is shown in Tables 7-8.

It is determined from the data presented in Tables 5, 6, 7 and 8 that when the specimen is under high rates of cooling, the maximum temperature of the points inside the column is lower than that of natural cooling. The reason for this is that the outer surface of the steel in the natural cooling takes a longer time to reach a temperature of 20($^{\circ}C$), and during this time the temperature of the interior points also increases gradually. However, in high rates of cooling, the surface temperature of the steel is rapidly decreased to 20($^{\circ}C$) while the concrete experiences a slight increase in temperature and then quickly enters the cooling phase.

In fact, during water cooling due to the higher cooling rate and the formation of micro-cracks in concrete, the residual strength of concrete is lower than the natural cooling. On the other hand, due to the high cooling rate and prevention of temperature increase in the internal points of the concrete in the early stages of cooling phase, the compressive strength of the specimen can be more than natural cooling, which will be investigated in the next section.

4.2 Natural cooling

After determining the temperature distribution of different points of the column, stress analysis is conducted to determine the mechanical behavior of the specimens according to section 2. In accordance with Tables 5, 6, 7, 8 to obtain post-fire residual strength, fire is stopped at 3 or 4 points and natural cooling is applied to the specimens using the Eq. (1). The curve of temperature variations at the heating and cooling phases is according to Fig. 1. The

Table 5 Temperature of selected points in the cross-section.

| Columns | Layers | Point | Maximum Temperature After 15 min (°C) | | Maximum Temperature After 30 min (°C) | | Maximum Temperature After 45 min (°C) | |
|----------------------|--------|-------------|---------------------------------------|-----|---------------------------------------|-----|---------------------------------------|-----|
| C1 C2 C4 C5 | 1 | A | 495 | | 669 | | 691 | |
| | | K | 525 | 508 | 669 | 664 | 713 | 700 |
| | | J(Steel) | 520 | | 663 | | 706 | |
| | | B(Steel) | 495 | | 655 | | 688 | |
| | 2 | j(concrete) | 336 | | 562 | | 630 | |
| | | B(concrete) | 220 | 215 | 394 | 412 | 480 | 500 |
| | | C | 120 | | 275 | | 365 | |
| | | I | 182 | | 416 | | 523 | |
| | 3 | C | 120 | | 275 | | 365 | |
| | | D | 73 | 121 | 212 | 299 | 300 | 397 |
| | | H | 107 | | 293 | | 400 | |
| | | I | 182 | | 416 | | 523 | |
| | 4 | D | 73 | | 212 | | 300 | |
| | | E | 62.5 | 80 | 185 | 227 | 270 | 320 |
| | | G | 74 | | 220 | | 310 | |
| | | H | 107 | | 293 | | 400 | |
| | 5 | E | 62.5 | | 185 | | 270 | |
| | | G | 74 | 63 | 220 | 187 | 310 | 285 |
| | | F | 56.8 | | 170 | | 250 | |

Table 6 Temperature of selected points in the cross-section.

| Columns | Layers | Point | Maximum Temperature After 10 min(°C) | | Maximum Temperature After 15 min(°C) | | Maximum Temperature After 20 min(°C) | |
|---------|--------|-------------|--------------------------------------|-----|--------------------------------------|-----|--------------------------------------|-----|
| C3 | 1 | A(Steel) | 332 | 332 | 446 | 445 | 553 | 550 |
| | | B(Steel) | 332 | | 443 | | 547 | |
| | 2 | B(concrete) | 250 | 215 | 326 | 280 | 395 | 341 |
| | | C | 180 | | 233 | | 286 | |
| | 3 | C | 180 | 154 | 233 | 201 | 286 | 246 |
| | | D | 128 | | 168 | | 205 | |
| | 4 | D | 128 | 112 | 168 | 146 | 205 | 178 |
| | | E | 95 | | 124 | | 151 | |
| | 5 | E | 95 | 88 | 124 | 115 | 151 | 141 |
| | | F | 81 | | 106 | | 130 | |
| | 6 | F | 81 | 80 | 106 | 105 | 130 | 128 |
| | | G | 78 | | 103 | | 126 | |

Residual strength of specimens at three or four time intervals are calculated with respect to the stability time of the specimens where According to Tables 5, 6, 7, 8, they are 15.30, 45, 60 min in specimens C1, C2, C4, C5, and 10, 15, and 20 min in specimen C3 with respect to its shorter stability time.

In order to study the effect of parameters such as the height of specimens, the strength of the material and cross-sectional shape, the axial load ratio for all specimens was assumed to be equal to 0.5, according to which different axial loads are obtained for each of the columns. In order to obtain the axial capacity of the specimens, Article 10 of Iranian National Building Requirements, which is in accordance with AISC is used. Fig. 9 shows the residual strength obtained from the specimens in Table 4 under natural cooling. The x-axis in Fig. 9 shows the duration of the specimens being exposed to fire and then the cooling phase begins.

As shown in Fig. 9, it is found that in specimen C3, with a circular cross-section, the residual strength of the specimen has increased in the cooling phase, but in other specimens the results are significant. In other specimens with square sections, the residual strength of the heating phase is higher for some of the specimens where in others, the residual strength of the cooling phase is higher. The reason that the residual strength is higher in the cooling phase is that the temperature of the internal points of the specimens is decreased and consequently the residual strength is increased. In some other specimens with high residual strength in the heating stage, the temperature of the inner layers increase when the outer layers cool down, and this increase in temperature causes the specimens to rupture.

The discussion here is that while the specimens are in the cooling phase, the internal layers are heated. It might be conceived at first that the cooling of the specimen will

Table 7 Temperature of selected points in the cross-section

| Columns | Layers | Point | Maximum Temperature After 15 min(°C) | | Maximum Temperature After 30 min(°C) | | Maximum Temperature After 45 min(°C) | |
|----------------------|--------|-------------|--------------------------------------|-----|--------------------------------------|-----|--------------------------------------|-----|
| C1 C2 C4 C5 | 1 | A | 495 | | 669 | | 692 | |
| | | K | 525 | 508 | 669 | 664 | 713 | 700 |
| | | J(Steel) | 520 | | 663 | | 706 | |
| | | B(Steel) | 492 | | 655 | | 688 | |
| | 2 | j(concrete) | 318 | | 530 | | 601 | |
| | | B(concrete) | 204 | 183 | 363 | 345 | 426 | 422 |
| | | C | 84 | | 192 | | 263 | |
| | | I | 124 | | 293 | | 398 | |
| | 3 | C | 84 | | 192 | | 263 | |
| | | D | 43 | 78 | 94 | 182 | 149 | 261 |
| | | H | 60 | | 148 | | 232 | |
| | | I | 124 | | 293 | | 398 | |
| | 4 | D | 43 | | 94 | | 149 | |
| | | E | 33 | 44 | 68 | 100 | 112 | 160 |
| | | G | 40 | | 89 | | 148 | |
| | | H | 60 | | 148 | | 232 | |
| | 5 | E | 33 | | 68 | | 112 | |
| | | G | 40 | 33 | 89 | 68 | 148 | 111 |
| | | F | 30 | | 57 | | 93 | |

Table 8 Temperature of selected points in the cross-section

| Columns | Layers | Point | Maximum Temperature After 10 min(°C) | | Maximum Temperature After 15 min(°C) | | Maximum Temperature After 20 min(°C) | |
|---------|--------|-------------|--------------------------------------|-----|--------------------------------------|-----|--------------------------------------|-------|
| C3 | 1 | A(Steel) | 306 | 306 | 450 | 445 | 550 | 549.5 |
| | | B(Steel) | 306 | | 440 | | 549 | |
| | 2 | B(concrete) | 138 | 119 | 228 | 200 | 308 | 279 |
| | | C | 100 | | 171 | | 250 | |
| | 3 | C | 100 | 72 | 171 | 120 | 250 | 173 |
| | | D | 44 | | 68 | | 95 | |
| | 4 | D | 44 | 38 | 68 | 55 | 95 | 75 |
| | | E | 31 | | 42 | | 56 | |
| | 5 | E | 31 | 29 | 42 | 38 | 56 | 49 |
| | | F | 27 | | 34 | | 43 | |
| | 6 | F | 27 | 26 | 34 | 34 | 43 | 42 |
| | | G | 26 | | 33 | | 41 | |

increase strength, though the increase of temperature inside the specimen can also lead to a decrease in residual strength. As seen from the specimens C1 and C4, the residual strength of the specimens has decreased in the cooling stage, but in specimens C2, C3, C5 in The natural cooling state, the residual strength is greater than that of corresponding values at the heating stage. As a result, the assumption that the residual strength of the specimen increases when cooling phase starts, cannot always be correct.

A significant point in confirming that the behavior of the CFST column at the cooling phase is not predictable is the buckling behavior of specimens in the failure mode as shown in Fig. 10. As in the case of specimens C2, C3, C5, where the residual strength in cooling phase is greater than that of the heating phase, The reason of failure is local buckling, so that the specimen can resist until the entire cooling phase is complete; but in specimens C1 and C4

where the residual strength in the heating phase is greater than the cooling phase, The reason of failure is the global buckling, and before the specimen is completely cold, the buckling occurs and the specimen is ruptured.

4.3 Water cooling

In the water cooling phase, due to the higher cooling rate, the mechanical behavior of the specimens is also different than natural cooling. The studies conducted by Li and Franssen (2011) have been used to consider the effect of cooling rate on the concrete properties. In this experimental study, several specimens have been subjected to natural cooling and water cooling and the results are presented in Fig. 11.

f =Residual strength of concrete for different cooling regimes

$f_c(20)$ =compressive strength of concrete at ambient

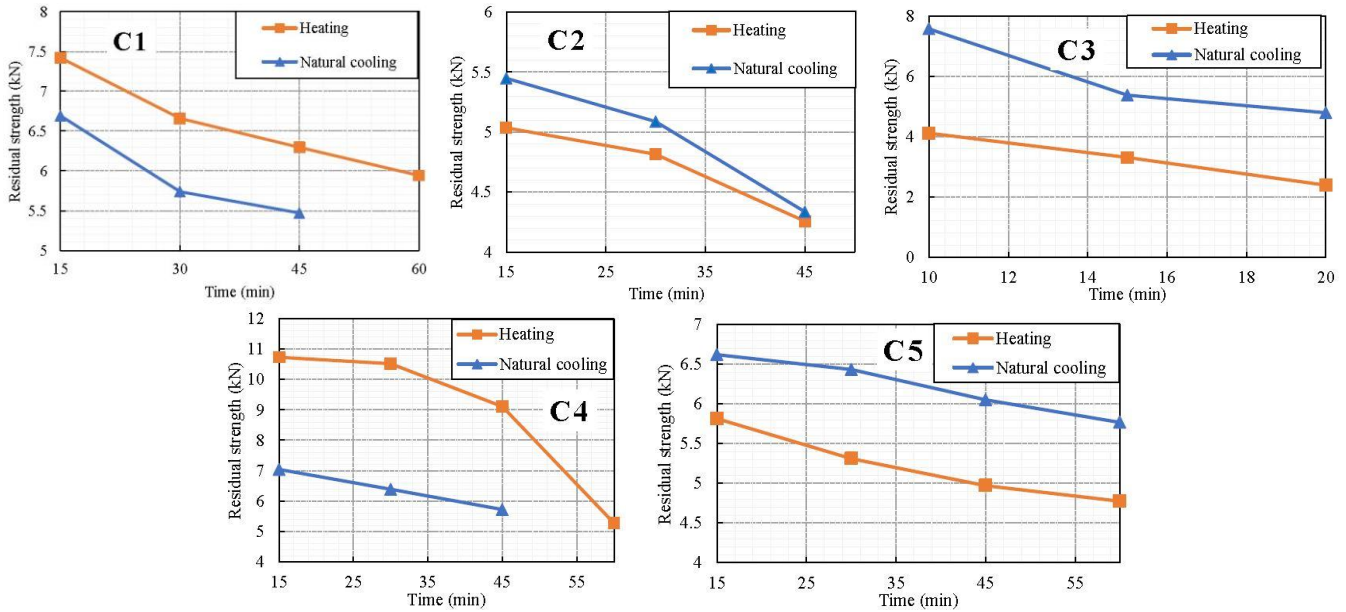


Fig. 9 Residual strength changes for the natural Cooling and heating phase

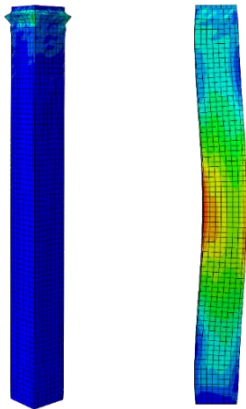


Fig. 10 Buckling patterns of specimens

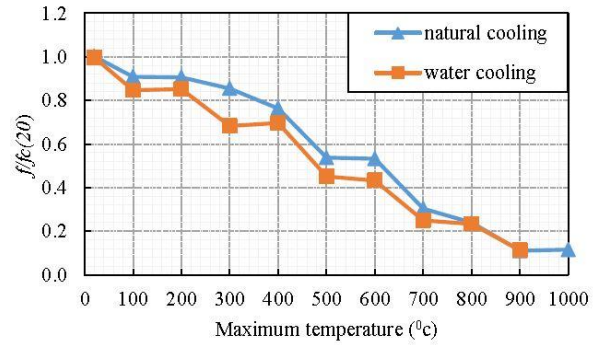


Fig. 11 Residual strength for different cooling regimes (Li and Franssen 2011)

temperature

Using Fig. 11, the compressive strength reduction ratio of water cooling to the natural cooling state can be obtained. By calculating the reduction ratio, compression strength can be obtained for water cooling at desired models. These values are in accordance with Table 9.

As for steel, relations proposed by Lu *et al.* (2016) were used to determine the yield strength variations and the elastic modulus. The elastic modulus and the yield strength are used via Eqs. (23) -(24).

$$\begin{cases} \frac{E_{PT}}{E} = 1 & 20 \leq T \leq 800 \text{ } ^\circ\text{C} \\ \frac{E_{PT}}{E} = 2.891 - 4.27 \times 10^{-3}T + 2.23 \times 10^{-6}T^2 & 800 \leq T \leq 1000 \text{ } ^\circ\text{C} \end{cases} \quad (23)$$

$$\begin{cases} \frac{f_{y,PT}}{f_y} = 1.007 + 2.17 \times 10^{-5}T & 20 \leq T \leq 600 \text{ } ^\circ\text{C} \\ \frac{f_{y,PT}}{f_y} = 1.313 - 4.75 \times 10^{-4}T & 600 \leq T \leq 1000 \text{ } ^\circ\text{C} \end{cases} \quad (24)$$

E_s =Steel modulus of elasticity (MPa)

f_y =Yield strength of steel at ambient temperature (MPa)

T =Temperature ($^\circ\text{C}$)

According to the assumption Dimia *et al.* (2011) the thermal properties of the concrete, including thermal conductivity and specific heat, change neither at the cooling phase nor in the case of water cooling and are equal to the corresponding values at their maximum temperature. Likewise, the thermal properties of steel return to their initial value at the cooling phase. In order to compare the effect of water cooling on the behavior of the CFST column, similar to natural cooling, the residual strength of the specimens is compared with each other according to Fig. 12. The x-axis in Fig. 12 shows the duration of the specimens being exposed to fire and then the cooling phase begins.

According to Fig. 12, it is also observed that with increasing the time of exposure of the specimens against fire, their residual strength decreases. Also, the results obtained in this section are similar to the results of natural cooling. The residual strength of the specimen C3 with a circular cross-section in the water cooling is higher than that of the heating phase. In specimens C1 and C4 with a

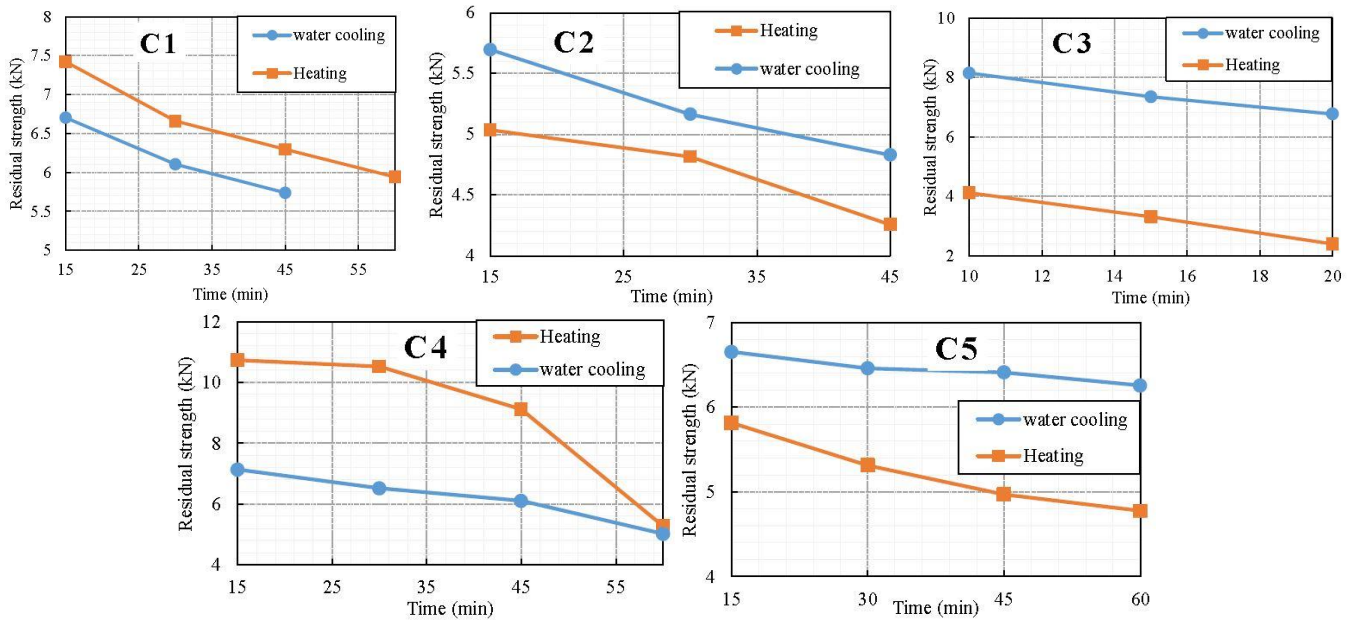


Fig. 12 Residual strength changes for the water Cooling and heating phase

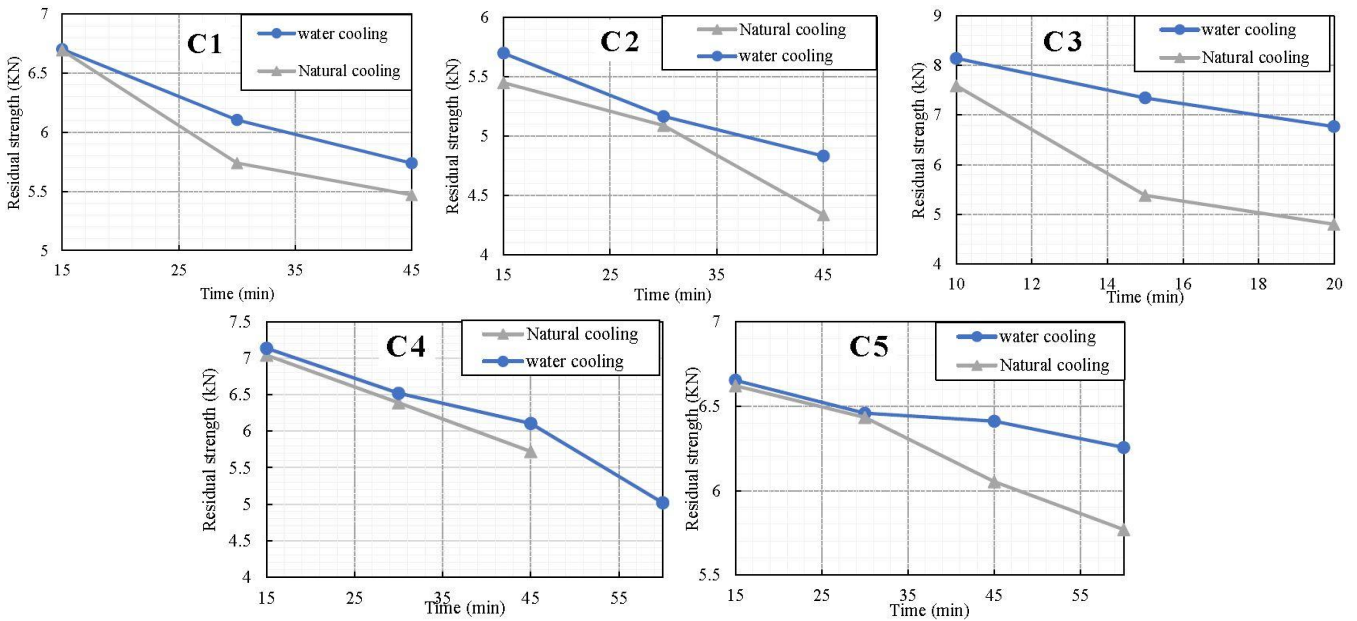


Fig. 13 Residual strength changes for the natural Cooling and water cooling phase

square section, due to the reasons given in section 4-2, water cooling has less residual strength as to heating stage. However, the residual strength of specimens C2 and C5 at the water cooling phase is more than the heating phase.

4.4 Comparing natural and water cooling

The effect of the cooling rate on the residual strength of the specimens according to Fig. 13 are compared. The x-axis in Fig. 13 shows the duration of the specimens being exposed to fire and then the cooling phase begins.

From Fig. 13 it is shown that the residual strength of the specimens decreases with the increase of the time during which specimens are exposed to fire. It is also observed that the residual strength in the case of natural cooling is less

than water cooling. Two sorts of issues are to be addressed affecting the results. The first is that, in the case of water cooling, the temperature of the points in the specimens is decreased faster than natural cooling, thus the residual strength of the concrete is more in this case. The second one is the rapid cooling of the concrete causes micro-cracks in the concrete, which reduces the compressive strength of the concrete.

The effect of these two phenomena together forms the behavior of the CFST column under different rates of cooling. By assessing the temperature of concrete points and their compressive strength, it was observed that increase of the compressive strength due to the rapid decrease of temperature surpassed the reduction of strength due to micro-cracks in the concrete. Consequently, the

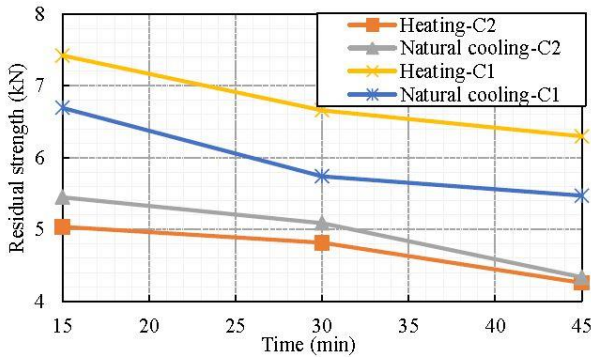


Fig. 14 Residual strength changes for the specimens C1 and C2

residual strength of the specimens under water cooling is more than the specimens under natural cooling. However, it should be noted that various parameters affect this issue. These include specimen's height, axial load ratio, steel and concrete strength, cross-sectional shape, etc. The following section evaluates the effects of the above-mentioned parameters.

5. Parametric analysis

5.1 The effect of material strength

In order to investigate the effect of steel and concrete strength on the residual strength of specimens under different cooling rates, specimens C1 and C2 were investigated. In this case, the axial load ratio is assumed to be constant. As a result, by decreasing the strengths of steel and concrete, the axial load applied to the column also decreases. According to Fig. 14, it can be seen that by decreasing the compressive strength of the concrete and the yield stress of the steel, the residual strength of the specimens in the cooling phase, is more than the heating phase due to the lower axial load in the specimen C2. The reason for this is that in specimen C2, although the strength in steel and concrete has decreased, because of the axial load reduction, the specimen can resist until the entire section is cooled.

Therefore, after the cooling phase, its residual strength is more than the heating phase. However, in the specimen C1, due to the higher axial load, the specimen is ruptured in the global buckling mode with a slight increase in the temperature at the cooling stage. Moreover, with the increasing strength of steel and concrete, the residual strength of the specimen C1 is also higher than that of C2.

It is resolved that once materials with higher strength are used instead of increasing the column dimensions in a multi-story building in which lower floors carry more loads, the residual strength of columns will be reduced in the cooling phase as to the heated column, thus resulting in failure. Accordingly, believing that columns on lower floors have adequate load bearing-capacity during the cooling phase is quite erroneous. The x-axis in Fig. 14 shows the duration of the specimens being exposed to fire and then the cooling phase begins.

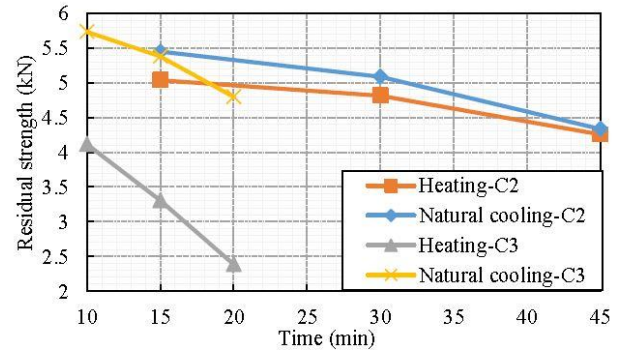


Fig. 15 Residual strength changes for the specimens C2 and C3

5.2 The effect of cross-sectional Shape

To investigate the effect of cross-sectional shape, specimen C2 with a square section and specimen C3 with a circular cross-section will be compared. In these two shapes, the load carrying capacity of the specimens was approximately equal, being 4838 kN in specimen C2 and 4867 kN in specimen C3. According to Fig. 15, it is observed that in the specimen C2 with a square section, the residual strength in the heating phase is greater than the cooling phase. However, in the specimen C3 with a circular cross-section, the residual strength is higher in the two cases of the cooling phase. The reason for this is that according to Fig. 15, the temperature distribution at circular cross-section is uniform, though it is higher in the corners at the square cross-section. As a result, the temperature of the internal points of the specimens at the cooling phase increases for a longer period of time, decreasing with a delay. Therefore, this section in the cooling phase has less residual strength than the heating phase.

The point to set forth here is that once the circular section is used in place of a square one, intended for aesthetic issues, etc., it is to be mentioned that the residual strength of such column increases in the cooling phase, resulting in a safer surrounding as to the square column. Consequently, employing circular cross-sectional columns are to opt for regarding their behavior at the cooling phase. The x-axis in Fig. 15 shows the duration of the specimens being exposed to fire and then the cooling phase begins.

5.3 The effect of specimen height

To investigate the height effect, the specimen C1 is compared with the specimen C4. In specimen C4, the height is reduced by half the initial value. In this case, since the axial load ratios are assumed equal, the axial load increased with decreasing height and thus reducing slenderness. From Fig. 16 it is observed that by decreasing the specimen height, there is no difference in the behavior of the specimens and, as in specimen C1, the residual strength of the heating stage is greater than that of the cooling phase. Since the column tends to behave as a short one, its residual strength increases both in the heating phase and the two cooling modes compared to specimen C1. As a significant point, in this case, there is a great difference between the

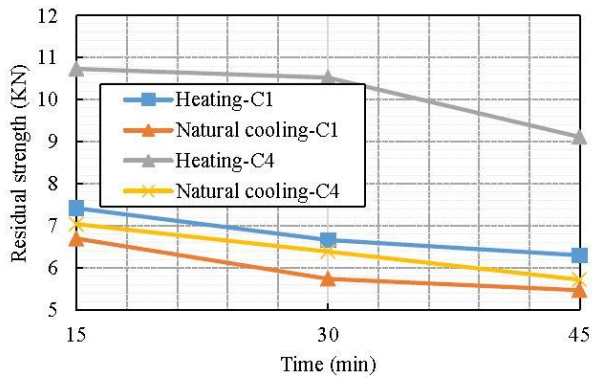


Fig. 16 Residual strength changes for the specimens C1 and C4

residual strength curves in the heating mode and the two cooling modes in specimen C4. The reason is the high efficiency of temperature increase inside the specimen at the cooling phase, which greatly reduces the residual strength. It is also observed from the curve attributed to specimen C4, that the residual strength of the specimens is very close to each other at the initial moments, though increases with increasing temperature. The rationale is compensating the effect of residual strength increase due to rapid water cooling for the strength reduction owing to micro-cracks in concrete, being lower at initial temperatures, yet gaining increase as temperature rises. The x-axis in Fig. 16 shows the duration of the specimens being exposed to fire and then the cooling phase begins.

5.4 The effect of load ratio

In order to evaluate the effect of axial load, specimens C1 are compared with the specimen C5. In specimen C5, as shown in Table 4, the axial load ratio is reduced to 0.35. According to Fig. 17, by reducing the axial load, the column's behavior will be such that it will not be ruptured until it is completely cooled. As a result, the post-fire residual strength of the specimens will be more than the heating phase. In this case, the effect of the cooling rate is low at low temperatures and will increase by increasing of temperature. The x-axis in Fig. 17 shows the duration of the specimens being exposed to fire and then the cooling phase begins.

6. Conclusions

According to the results obtained from this study, it was determined:

- In the course of cooling of interior columns of the building, one cannot always suppose that the residual strength of the member will increase and the column after the fire will still be safe. It is possible that the column is failed during the cooling phase, leading to the collapse of the structure.
- It cannot be precisely predicted that cooling the column at a higher rate, for example with water, or at lower rates such as natural cooling, will have a positive

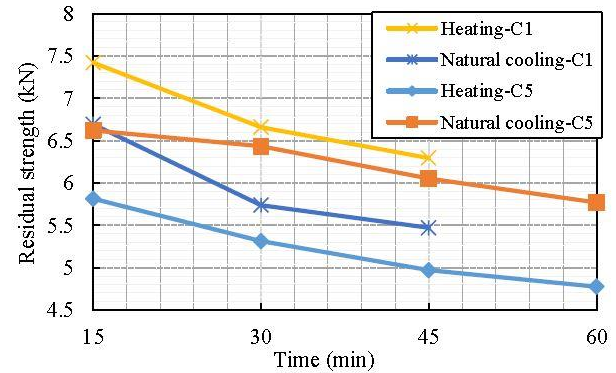


Fig. 17 Residual strength changes for the specimens C1 and C5

or negative effect on the column behavior. The rapid cooling causes micro-cracking of the concrete and, on the other hand, reduces the temperature in the specimen faster. The interaction between these two factors will determine the behavior of the column in the cooling phase with different rates. In this study, the residual strength in water cooling is more than natural cooling. In addition, with increasing temperature, the difference between the responses of different cooling rates will increase.

- By increasing the steel and concrete strengths as well as the column axial load ratio, the residual strength in the cooling phase is less than that of the heating phase. Moreover, there is no change in the post-fire behavior of column with reducing the column height.
- By changing the cross-sectional shape of the columns from square to circular, the post-fire residual strength is greater than that of the heating phase. As a result, under equal conditions, the use of circular columns is better because of its more appropriate behavior.

References

- Abbas, H., Al-Salloum, Y., Alsayed, S., Alhaddad, M. and Iqbal, R. (2017), "Post-heating response of concrete-filled circular steel columns", *KSCE J. Civil Eng.*, **21**(4), 1367-1378.
- Abdollahzadeh, G.H. and Afaghi, D.A. (2017), "Effect of drywall and brick wall on fire behavior of concrete-filled steel tube column", *Struct. Concrete*, **19**(3), 851-863.
- Abdollahzadeh, G.H. and shalika, R. (2017), "Retrofitting of steel moment-resisting frames under fire loading against progressive collapse", *Int. J. Steel Struct.*, **17**(4), 1597-1611.
- Abramowicz, M. and Kowalski, R. (2005), "The influence of short time water cooling on the mechanical properties of concrete heated up to high temperature", *J. Civil Eng. Manage.*, **11**(2), 85-90.
- Anderberg, Y. and Thelandersson, S. (1976), "Stress and deformation characteristics of concrete at high temperatures. 2. experimental investigation and material behaviour model", *Bulletin of Division of Structural Mechanics and Concrete Construction*, Bulletin 54.
- BS-476-20 (1987), *Fire Tests on Building Materials and Structures Method for Determination of the Fire Resistance of Elements of Construction (General Principles)*.
- Chen, J., Young, B. and Uy, B. (2006), "Behavior of high strength

- structural steel at elevated temperatures”, *J. Struct. Eng.*, **132**(12), 1948-1954.
- Dimia, M.S., Guenfoud, M., Gernay, T. and Franssen, J.M. (2011), “Collapse of concrete columns during and after the cooling phase of a fire”, *J. Fire Protec. Eng.*, **21**(4), 245-263.
- Dimia, M.S., Guenfoud, M., Gernay, T. and Franssen, J.M. (2011), “Collapse of concrete columns during and after the cooling phase of a fire”, *J. Fire Protec. Eng.*, **21**(4), 245-263.
- Dimia, M.S., Sekkiou, S., Baghdadi, M. and Guenfoud, M. (2017), “Structural behaviour of concrete filled hollow steel sections exposed to parametric fire”, *Challenge*, **3**(4), 160-165.
- Ding, J. and Wang, Y.C. (2008), “Realistic modelling of thermal and structural behaviour of unprotected concrete filled tubular columns in fire”, *J. Constr. Steel Res.*, **64**(10), 1086-1102.
- Eurocode 1 (2002), Actions on Structures-Part 1-2: General Actions-Actions on Structures Exposed to Fire, British Standards Institution.
- Gernay, T. and Dimia, M.S. (2011), “Structural behavior of concrete columns under natural fires including cooling down phase”, *Proceedings of The International Conference on Recent Advances in Nonlinear Models-Structural Concrete Applications*, 637-656.
- Gernay, T. and Dimia, M.S. (2013), “Structural behaviour of concrete columns under natural fires”, *Eng. Comput.*, **30**(6), 854-872.
- Ghojel, J. (2004), “Experimental and analytical technique for estimating interface thermal conductance in composite structural elements under simulated fire conditions”, *Exp. Therm. Fluid Sci.*, **28**(4), 347-354.
- Gourley, B.C., Tort, C., Dennavit, M.D., Schiller, P.H. and Hajjar, J.F. (2001), “A synopsis of studies of the monotonic and cyclic behavior of concrete-filled steel tube beam-columns”, ST-01-4, Institute of Technology University of Minnesota.
- Guergah, C., Dimia, M.S. and Guenfoud, M. (2018), “Contribution to the numerical modelling of the spalling phenomenon: Case of a reinforced concrete beams”, *Arab. J. Sci. Eng.*, **43**(4), 1747-1759.
- Han, L.H. (2001), “Fire performance of concrete filled steel tubular beam-columns”, *J. Constr. Steel Res.*, **57**(6), 697-711.
- Han, L.H., Yang, H. and Cheng, S.L. (2002), “Residual strength of concrete filled RHS stub columns after high temperatures”, *Adv. Struct. Eng.*, **5**(2), 123-134.
- Han, L.H., Yang, Y.F. and Xu, L. (2003), “An experimental study and calculation on the fire resistance of concrete-filled SHS and RHS columns”, *J. Constr. Steel Res.*, **59**(4), 427-452.
- Ibrahimbegovic, A., Boulkertous, A., Davenne, L., Muhasilovic, M. and Pokrklic, A. (2010), “On modeling of fire resistance tests on concrete and reinforced-concrete structures”, *Comput. Concrete*, **7**(4), 285-301.
- Li, Y.H. and Franssen, J.M. (2011), “Test results and model for the residual compressive strength of concrete after a fire”, *J. Struct. Fire Eng.*, **2**(1), 29-44.
- Liang, J.F., Wang, E., Zhou, X. and Le, Q.L. (2018), “Influence of high temperature on mechanical properties of concrete containing recycled fine aggregate”, *Comput. Concrete*, **21**(1), 87-94.
- Liang, J.F., Yang, Z.P., Yi, P.H. and Wang, J.B. (2017), “Stress-strain relationship for recycled aggregate concrete after exposure to elevated temperatures”, *Comput. Concrete*, **19**(6), 609-615.
- Lie, T.T. (1994), “Fire resistance of circular steel columns filled with bar-reinforced concrete”, *J. Struct. Eng.*, **120**(5), 1489-1509.
- Lie, T.T. and Chabot, M. (1992), “Experimental studies on the fire resistance of hollow steel columns filled with plain concrete”, NRC-IRC-4196, National Research Council Canada.
- Lie, T.T. and Irwin, R.J. (1995), “Fire resistance of rectangular steel columns filled with bar-reinforced concrete”, *J. Struct. Eng.*, **121**(5), 797-805.
- Lu, J., Liu, H., Chen, Z. and Liao, X. (2016), “Experimental investigation into the post-fire mechanical properties of hot-rolled and cold-formed steels”, *J. Constr. Steel Res.*, **121**, 291-310.
- Outinen, J. and Mäkeläinen, P. (2004), “Mechanical properties of structural steel at elevated temperatures and after cooling down”, *Fire Mater.*, **28**(2-4), 237-51.
- Ozbolt, J., Periskic, G., Reinhardt, H.W. and Eligehausen, R. (2008), “Numerical analysis of spalling of concrete cover at high temperature”, *Comput. Concrete*, **5**(4), 279-293.
- Peng, G., Nakamura, S., Zhu, X., Wu, Q. and Wang, H. (2017), “An experimental and numerical study on temperature gradient and thermal stress of CFST truss girders under solar radiation”, *Comput. Concrete*, **20**(5), 605-616.
- Sakumoto, Y., Okada, T., Yoshida, M. and Tasaka, S. (1994), “Fire resistance of concrete-filled, fire-resistant steel-tube columns”, *J. Mater. Civil Eng.*, **6**(2), 169-184.
- Song, T.Y., Han, L.H. and Yu, H.X. (2010), “Concrete filled steel tube stub columns under combined temperature and loading”, *J. Constr. Steel Res.*, **66**(3), 369-384.
- Tan, Q., Gardner, L. and Han, L.H. (2018), “Performance of steel-reinforced concrete-filled stainless steel tubular columns at elevated temperature”, *Int. J. Struct. Stab. Dyn.*, **19**(1), 1940002.
- Yang, H., Han L.H. and Wang, Y.C. (2008), “Effects of heating and loading histories on post fire cooling behaviour of concrete filled steel tubular columns”, *J. Constr. Steel Res.*, **64**(5), 556-570.
- Yang, H., Liu, F. and Gardner, L. (2013), “Performance of concrete-filled RHS columns exposed to fire on 3 sides”, *Eng. Struct.*, **56**, 1986-2004.
- Yao, Y. and Hu, X.X. (2015), “Cooling behavior and residual strength of post-fire concrete filled steel tubular columns”, *J. Constr. Steel Res.*, **112**, 282-292.
- Yu, M., Zha, X., Ye, J. and Li, Y. (2010), “Fire response and resistance of concrete-filled steel tubular frame structures”, *Int. J. Struct. Stab. Dyn.*, **10**(2), 253-271.
- Zhang, J.B., Xu, Z.D., Han, J.S. and Wang, X.D. (2011), “Prediction of the thermal contact resistance at the steel-concrete interface of CFST columns with circular cross-section”, *Mech. Adv. Mater. Struct.*, **19**, 530-542.

CC